Spring 5-9-2020

Crystallization Efforts for an Engineered Nickel-Binding Protein, Gold-Bovine Serum Albumin Nanoclusters, and an Artificial De Novo Tetramer Hydrogenase Mimic

Skyler Crane

Crystallization Efforts for an Engineered Nickel-Binding Protein, Gold-Bovine Serum Albumin Nanoclusters, and an Artificial De Novo Tetramer Hydrogenase Mimic

By

Skyler Crane

A thesis submitted to the faculty of The University of Mississippi in partial fulfillment of requirements of the Sally McDonnel Barksdale Honors College

Oxford

April 2020

Approved by:

_____

Advisor: Professor Saumen Chakraborty

_____

Reader: Professor Jared Delcamp

_____

Reader: Professor Susan Pedigo

ACKNOWLEDGEMENTS

The Sally McDonnell Barksdale Honors College

The University of Mississippi, Chemistry Department

The Chakraborty Lab

Dr. Chakraborty

Dr. Delcamp

Dr. Pedigo

ABSTRACT

Skyler Crane: Crystallization Efforts for an Engineered Nickel-Binding Protein, Gold-Bovine Serum Albumin Nanoclusters, and an Artificial Hydrogenase Mimic

(Under the direction of Dr. Saumen Chakraborty)

Protein crystallization is fundamental to modern research efforts given its ability to determine a protein's structure as well as the interactions that structure allows and relies upon. This process, though lacking direct application, provides necessary information for subsequent research efforts for which applications may be explored. As such, efforts were taken to crystallize nickel-binding protein (NBP) reengineered from Copper Storage Protein 1 (Csp1) in its apo and metal bound form, Bovine Serum Albumin (BSA) in its apo and gold bound form (Au-BSA), and an artificial de novo tetramer hydrogenase mimic peptide to better inform future research actions for these respective molecules. Efforts yielded apo-NBP crystals of sufficient quality from which a structure could be determined. Apo-BSA crystals were formed; however, their morphology was unsuitable for structure determination. Au-BSA, Ni-NBP, and the de novo tetramer currently are undergoing condition optimization to more efficiently develop crystals for structure elucidation.

Table of Contents

List of Figures

List of Equations

Chapter 1: Introduction

1.1 Bragg's Law

Max von Lane's initial use of x-rays on crystal structures in 1912 gradually metamorphosized into the modern science of crystallography.[1] Crystallography is used to deduce the structure of a material of interest as it is in a solid, crystalline form by studying the patterns formed when incident x-rays diffract off of atoms in a material and interact with other diffracted x-rays.[2] This process assists in the elucidation of the relationship between that material's properties and structure. As such, crystallography is used for tasks ranging from soil analysis[3] to small molecule imaging.[4,5] An application of this method relevant to protein structure elucidation was John Kendrew and Max Perutz's determination of myoglobin's structure,[6] an act that saw the duo awarded the 1962 Nobel prize in chemistry and catalyzed subsequent protein crystallization efforts.

To expand on previous statements, crystallography uses the angles and intensities resulting from the interactions of diffracted x-rays to determine electron density inside the crystal which can then be used to determine atomic bond lengths and angles. This is feasible via the following observation: When x-rays enter a crystal, they scatter off of the sample's atoms to interfere with other scattered x-rays similar to how a shore wall breach causes waves to knock against one another.[7] This phenomenon was later algebraically expressed as Bragg's Law provided in **Eq. 1** and visually simulated in **Figure 1**.

$$n\lambda = 2d \sin\theta \ldots\ldots \text{Eq. 1}$$

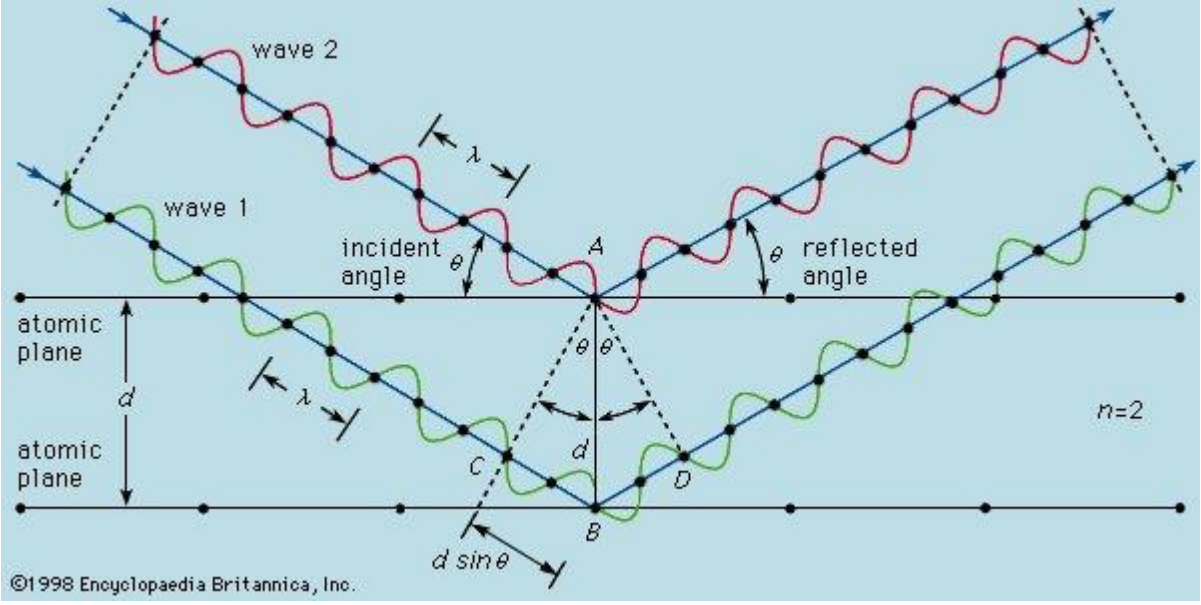

Figure 1: A diagram depicting a lattice adhering to Bragg's Law.[8]

Bragg's Law's variables are defined as follows: n = a whole number of wavelengths along path CBD as shown in **Figure 2** (i.e. order of reflection), λ = the incident ray's wavelength, d = the distance between the crystal's lattice planes, and θ = the angle of reflection.[2] Bragg's Law is applicable to instances of constructive interference and elastic light scattering. Deviations from these conditions results in its mathematic expression being rendered irrelevant. For instance, if n were a fraction, the corresponding θ value would cause destructive interference with the reflected wavelength thus destroying it and rendering a diffraction pattern unobservable.

1.2 Generalized Crystallization Procedure(s)

This information, though useful, does not describe how to create a crystal for which this phenomenon can be applied. Considering this work's focus, subsequent discussion of crystallization will correlate most closely with proteins and protein-metal complexes. A general outline for protein crystallization is detailed here. The pure protein is either commercially acquired or prepared via transforming the gene that codes the desired protein into a bacterium, stimulating

that gene's expression, then purifying that desired protein from the resulting supernatant following centrifugation of the bacterial cultural. From there, a variety of conditions are tested ("screened") to optimize the system's (i.e. mother liquor's) components. The conditions deemed most promising are then further optimized via trial and error to create parameters that result in the most well-developed crystals. The crystals are then extracted from the mother liquor and exposed to x-ray diffraction techniques so the protein's structure can be determined by software analysis. This process is visualized in **Figure 2**.

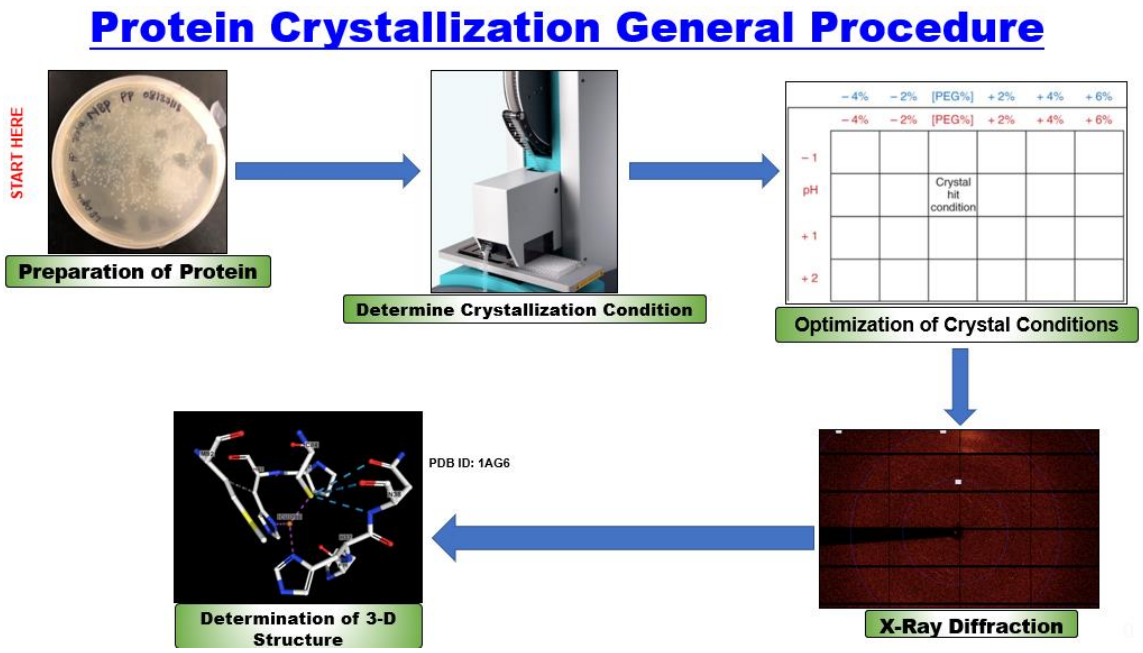

Figure 2: Visualization of general crystallization procedure. Note the structure presented here is not from this study and is there for demonstrative purposes

Additionally, it is necessary to address the fundamentals involved with protein crystal formation. Any crystal morphology descriptors are mimicked from professional practice.[9] Crystal formation is divided into two distinct steps: nucleation and growth. Nucleation is the transition of protein molecules into an ordered state known as a critical nucleus from an unordered state, and growth is the expansion of the critical nucleus via "dislocation growth" and "growth by two-dimensional nucleation" phenomena[10,11] which is *thought* to result from statistical fluctuations in

a solution's properties.[1,12,13,14] What is *known*, however, is crystal formation requires a supersaturated environment. This observation is visualized in **Figure 3**.

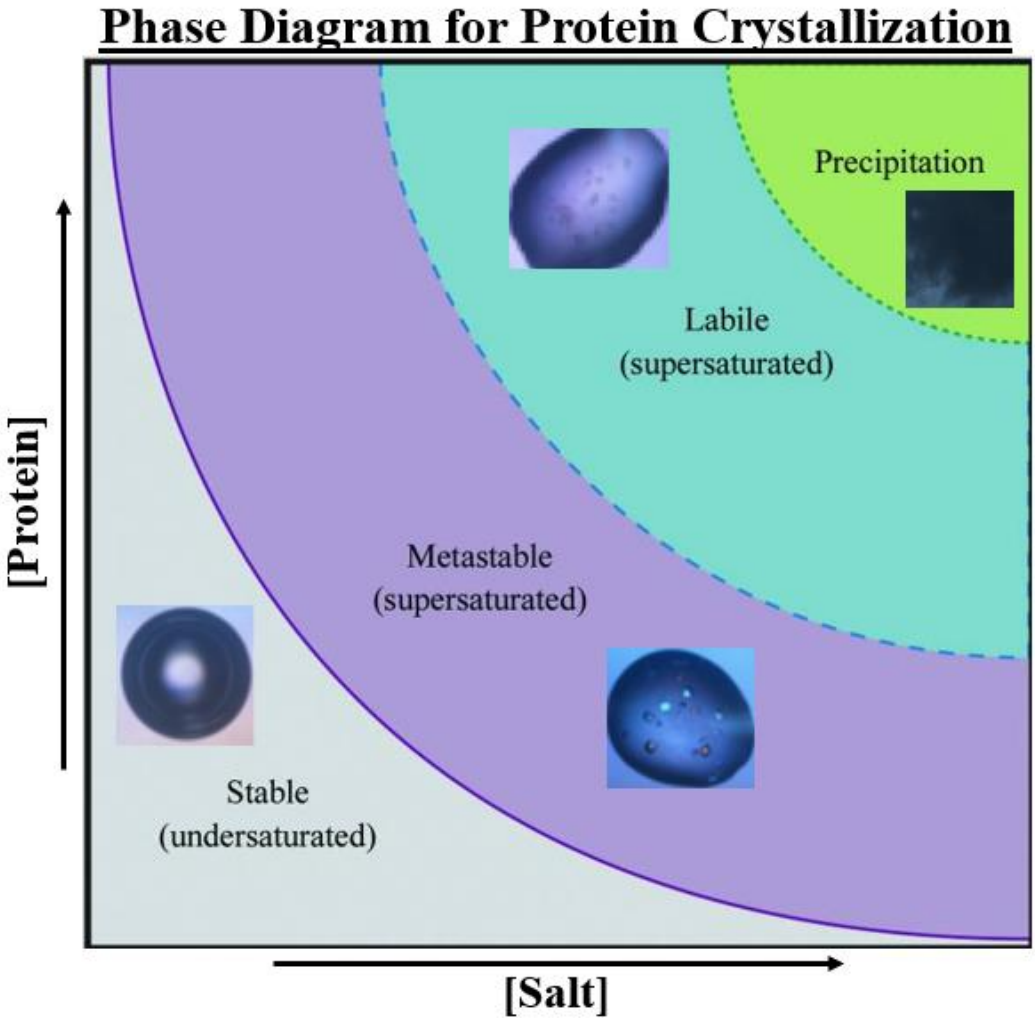

Figure 3: A generic phase diagram detailing conditions for crystallization. Borders between subareas indicate a state of equilibrium in the mother liquor

As can be seen in **Figure 3**, the more ideal crystal morphologies are more likely to form in supersaturated conditions with examples being the sharp-angled single crystals seen in the figure's Metastable region and the quasi crystals, perhaps microcrystals, shown in the Labile region. If the protein and salt concentrations are too high, precipitation occurs preventing crystal formation, and not including enough protein or salt results in an uneventful solution. As can also be noted in

Figure 3, the range for supersaturation is broad and therefore differs depending on the crystal species further reinforcing the importance of mother liquor condition optimization.

Protein crystallography methods must consider the nature of proteins, namely that they largely coevolved in living systems based on aqueous chemistry bounded by specific pH and temperature parameters from which deviation equates to destruction.[1,12] Additionally, protein crystals typically are more fragile than crystals of other molecule types due to their large size and complexity exasperating the consequences of conformational dynamics (i.e. polymorphism) based on Anfinsen's dogma.[4] They also diffract x-rays poorly due to relatively low degrees of internal order and the existence of solvent regions[1] and are damaged by extended exposure to electromagnetic radiation.[1] Therefore, even when the mother liquor's conditions are appropriate for a protein, protein crystals tend to develop to different degrees even when said conditions are replicated rendering their structures indecipherable by software such as CCP4, Phenix, and Molrep. Thus, this phenomenon requires even more numerous replications of the same condition to determine with increased certainty that condition's viability. This can be accomplished in many ways, but this discussion will be limited to two methods due to their relevance to this work: hanging drop vapor diffusion and sitting drop vapor diffusion. Schematics for each method are provided in **Figure 4**[15] and **Figure 5**[15] respectively.

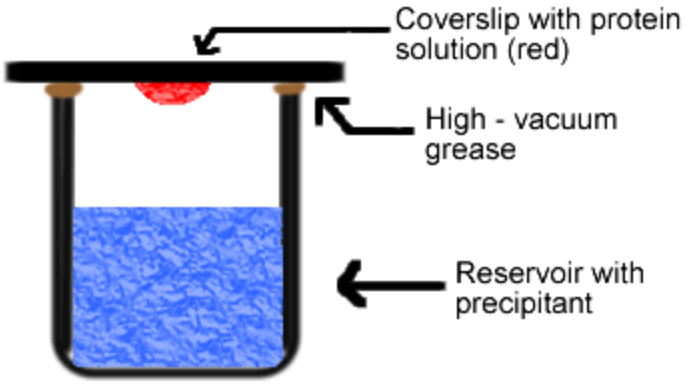

Figure 4: Diagram of the hanging drop method where the reservoir solution (blue) typically is composed of precipitant and buffer, and the protein solution (red) contains the same components in lower concentrations as well as trace metals or ions necessary for precipitation.

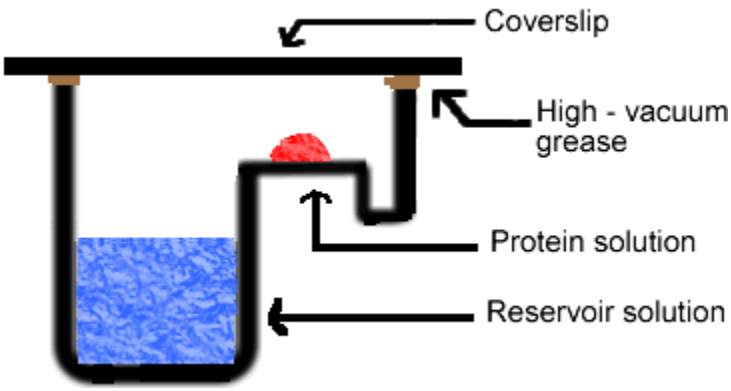

Figure 5: Diagram of the sitting drop method where conditions are identical to the hanging drop method except the protein drop sits on a dais above the reservoir solution instead of hanging from the coverslip.

Both methods depicted above use the same principles and differ only by the orientation of the drop. An aqueous solution of protein, buffer, and precipitate and a reservoir solution made of the same components minus the protein is created and isolated as a closed system by high-vacuum grease. Within this closed system, the reservoir solution contains a higher concentration of precipitate than the protein solution causing an imbalance in water distribution which is solved by diffusion of water into the reservoir solution to restore the system's equilibrium. This results in the protein solution's protein concentration gradually increasing thereby increasing the probability of crystallization. These systems test for a single set of conditions which can then be replicated as

needed. Typically, these systems are confined to “wells” in a tray-like apparatus alongside other systems to allow for more effective condition screening. One “tray” configuration that is used in this work is shown in **Figure 6**.

Figure 6: One of the trays used in this work. It is composed of a plastic 6 x 4 well system with a plastic cover. Note that the plastic cover is not the coverslip for the wells but it rather a protective shell to isolate the glass coverslips from damage.

This work applied these methods and their associated variable manipulations to crystallization efforts of apo-nickel binding protein (apo-NBP), its nickel-bound form (Ni-NBP), apo-bovine serum albumin (apo-BSA), its gold-bound form (Au-BSA), and an artificially-synthesized de novo tetramer hydrogenase mimic. Additional efforts were made to also purify nitrobindin heme protein (NBHP).

1.3 Nanoclusters

Considering the formation of metal-protein complexes, discussion of nanoclusters is required to frame this work's results. Nanoclusters are defined as submicroscopic particles ranging in size from less than one nanometer to two-point-two nanometers (**Figure 7**).[16]

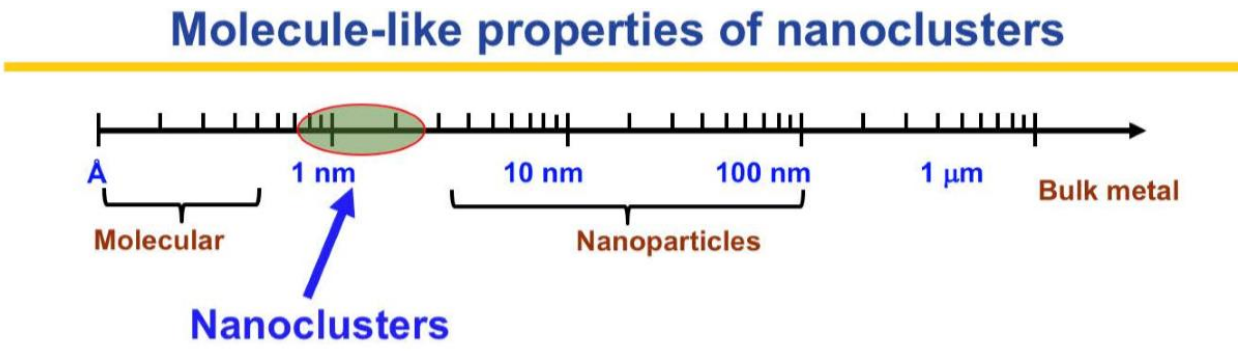

Figure 7: Visualization of nanocluster size alongside other submicroscopic particle categories for scale.

Nanoclusters have unique properties compared to larger nanoparticles leading scientists to speculate that these complexes have applications as energy production catalysts and biological labeling/sensing agents -- characteristics shared by gold nanoclusters.[17,18]

The work enclosed is basic scientific research with no direct applications; however, its conductance provides greater insight into the relationships between NBP's, NBHP's, BSA's, and THE DE NOVO TETRAMER'S respective structures, properties, and inter/intramolecular interactions. This, in turn, allows for more thorough investigations into potential applications for

the molecules listed. In short, this work is an intermediary - a bridge of sorts - needed to direct future research efforts.

Chapter 2: NBP

2.1 NBP Background

NBP is an artificial hydrogenase mimic reengineered from Copper storage protein 1 (Csp1) derived from bacteria *Methylosinus trichosporium* OB3b (PDB 5FJE).[19,20] NBP's tetramer structure differs from Csp1's by fifteen mutations: Nine cysteine [Cys] residues were mutated to seven alanine [Ala], one leucine [Leu], and one valine [Val] residues respectively; and six histidine [His] residues were modified into three glutamine [Gln] and three asparagine [Asn] residues. The Ala residues' purpose was to retain the protein's compact helical structure given its similar size to the replaced Cys residues (Cys33, Cys37, Cys51, Cys90, Cys106, Cys110, and Cys117), and the purpose of the Leu and Val residues (previously Cys103 and Cys94 respectively) was to provide hydrophobic packing to ensure the protein remained well-folded. As for the Gln and Asn residues, their purpose was to prevent Ni-binding competition by being noncoordinating whilst retaining the previous residues' polarity. Csp1's gene sequence is provided in **Figure 8**, its corresponding amino acid sequence is provided in **Figure 9**, and the gene and residue sequence modifications conducted for NBP's creation are provided in **Figure 10** and **Figure 11** respectively. **Figure 12** provide 3D models for Csp1 and NBP.

CATATG
TGGAGCCACCCGCAGTTCGAGAAGGGTGGCAGCGGTGAAGACCCGCACGCGGGCCA
CAAAATGAGCCACGGTGCGAAGTACAAAGCGCTGCTGGACAGCAGCAGCCACTGCG
TGGCGGTTGGTGAAGATTGCCTGCGTCACTGCTTTGAAATGCTGGCGATGAACGACG
CGAGCATGGGTGCGTGCACCAAGGCGACCTATGATCTGGTGGCGGCGTGCGGTGCG
CTGGCGAAACTGGCGGGTACCAACAGCGCGTTCACCCCGGCGTTTGCGAAGGTGGT
TGCGGACGTTTGCGCGGCGTGCAAGAAAGAGTGCGATAAGTTCCCGAGCATCGCGG
AGTGCAAAGCGTGCGGTGAAGCGTGCCAAGCGTGCGCGGAGGAATGCCACAAAGTG
GCGGCGTAA
CCATGG

Figure 8: The gene sequence for Csp1 is labeled in uncolored script. Restriction sites NdeI and NcoI are labeled in cyan and gray respectively. The stop codon is labeled in red.

WSHPQFEKGGSGEDPHAGHKMSHGAKYKALLDSSSHCVAVGEDCLRHCFEMLAMND
ASMGACTKATYDLVAACGALAKLAGTNSAFTPAFAKVVADVCAACKKECDKFPSIAE
CKACGEACQACAEECHKVAA

Figure 9: The primary sequence for Csp1 is labeled in uncolored script. The Strep Tag residues in yellow renders affinity chromatography capable of purifying NBP. A spacer sequence is labeled in violet. Cys residues are printed in red.

CATATG
TGGAGCCATCCGCAGTTTGAGAAGGGTGGTAGCGGTGAAGATCCGAACGCGGGTCA
GAAAATGAGCCAAGGTGCGAAATACAAGGCGCTGCTGGACAGCAGCAGCCAGTGC
GTGGCGGTTGGCGAGGATGCGCTGCGTAACGCGTTCGAAATGCTGGCGATGAACGA
TGCGAGCATGGGCGCGGCGACCAAAGCGACCTACGATCTGGTGGCGGCGTGCGGTG
CGCTGGCGAAACTGGCGGGTACCAACAGCGCGTTCACCCCGGCGTTTGCGAAAGTG
GTTGCGGATGTGTGCGCGGCGGCGAAGAAAGAGGTTGATAAATTTCCGAGCATCGC
GGAACTGAAAGCGGCGGGCGAAGCGGCGCAGGCGTGCGCGGAAGAAGCGAATAAA
GTGGCGGCGTAA
CCATGG

Figure 10: The gene sequence for NBP is labeled in uncolored script. Restriction sites NdeI and NcoI are labeled in cyan and gray respectively. The stop codon is labeled in red.

WSHPQFEKGGSGEDPNAGQKMSQGAKYKALLDSSSQCVAVGED LRN FEMLAMND
ASMGA TKATYDLVAACGALAKLAGTNSAFTPAFAKVVADVCAA KKE DKFPSIAE
KA GEA QACAEE NKVAA

Figure 11: The primary sequence for NBP is labeled in uncolored script. The Strep Tag residues in yellow renders affinity chromatography capable of purifying NBP. A spacer sequence is labeled in violet. Cys residues forming the Ni-binding site are highlighted in red. Residues modified from His are labeled in orange, and residues modified from Cys are labeled in white.

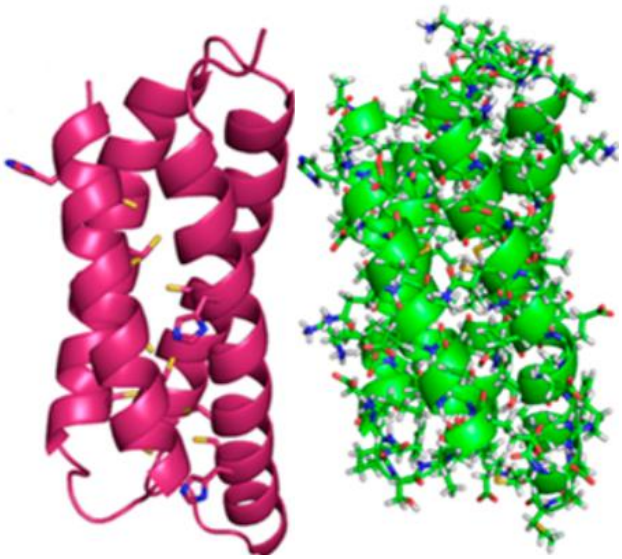

Figure 12: 3D models for Csp1 (right) and NBP (left). Models were created in NAMD using CHARMM22 force fields.

The remaining four Cys residues [Cys26, Cys62, Cys87, and Cys113] in **Figure 11** were retained so each α-helix had one Cys residue to form NBP's Ni-binding site. This binding site is visible in **Figure 13**.

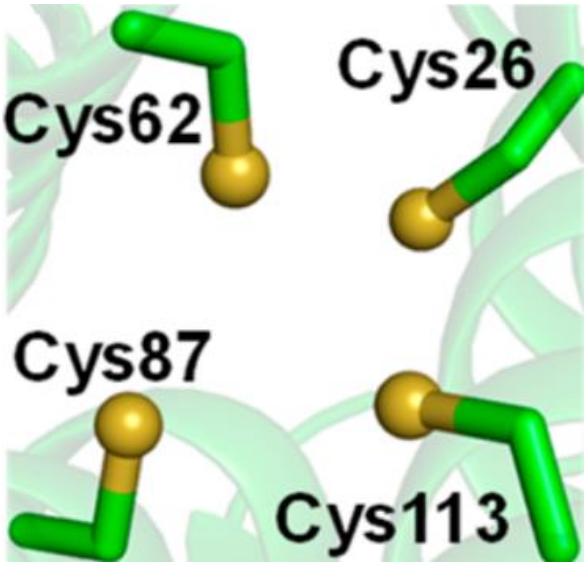

Figure 13: NBP's nickel binding site. Model was created using CHARM22 force fields

Additionally, a variant of NBP with no Cys residues was also created to ensure the absence of nickel binding. The Cys positions and residue mutations for this variant were as follows: Cys26→Ala, Cys62→Val, Cys87→Ala, and Cys113→Val.

2.2 NBP Expression and Purification Procedure

The procedure for NBP expression was as follows: A synthetic NBP gene with a N-terminal Strep-tag and GGS spacer (Genscript) was cloned into a pET 29a (+) vector at its NdeI/NcoI restriction sites. The gene was dissolved at 100 ng/µL in Milli-Q water and stored at −20°C. 50 µL of E.cloni EXPRESS DUOs BL21(DE3) chemically competent cells (Lucigen) was added to 1 µL of NBP gene in a 10 mL culture tube and incubated on ice for 30 minutes. The cells were then subjected to heat shock at 42°C for 45 seconds and further incubated in ice for 10 minutes. Cells were recovered with 1 mL of LB media in an incubator-shaker (Thermo Fisher MAXQ 4000) at 37°C for 1 hour. 50 µL of the cells were then plated on kanamycin LB agar plates (**Figure 14**) and incubated overnight at 37°C.

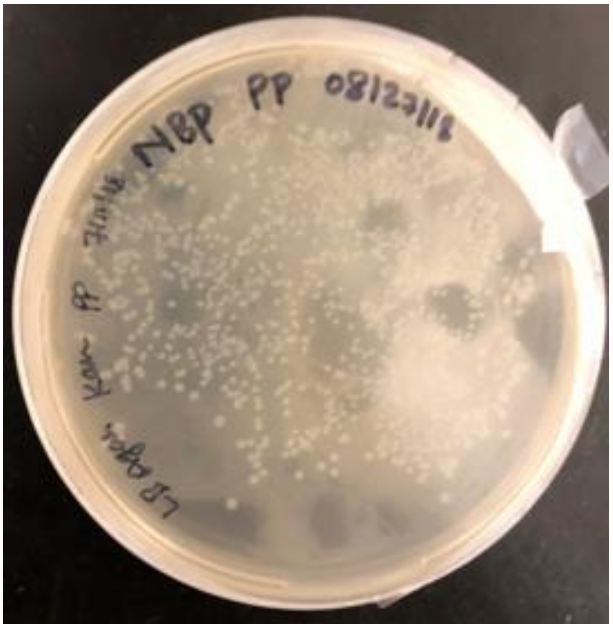

Figure 14: Representative LB Agar plate used for protein expression

10 mL primary cultures in LB media supplemented by 50 mg/mL kanamycin (Fisher) were inoculated with single colonies and grown overnight at 180 rpm at 37°C using the same incubator-shaker as previously described. 1 L of secondary culture in LB media supplemented by kanamycin was inoculated with 10 mL of primary culture and grown for 3-4 hours at 180 rpm at 37°C until

an optical density at 600 nm (OD_{600}) reached approximately 0.55. The cultures were then induced with 1 mM (final concentration) of isopropyl β-D-1-thiogalactopyranoside (IPTG; Goldbio). The induced culture was then allowed to grow for six hours at 180 rpm at 30°C. 10 mL of uninduced culture was grown, pelleted, and sonicated under conditions similar to those of the induced culture and then checked as a control on the gel. The cells were harvested at 6000 rpm (SORVALL RC 5B PLUS; **Figure 15**) for 10 minutes, and the pellets were stored in −20°C overnight.

Figure 15: Picture representative of cells harvested at 6000 rpm

The following day, the pellets were resuspended in 50 mL of lysis buffer consisting of 20 mM tris(hydroxymethyl)aminomethane (Tris-HCl; VWR) pH 8.5, 1 mM dithiothreitol (DTT; VWR), 1 mM phenylmethane sulfonyl fluoride (PMSF; Biosynth Inc.), 1 mM EDTA, and 10 μg/mL deoxyribonuclease (DNase I; Worthington Biochemical Corp.) followed by sonication on ice (Branson) for 3 minutes using a 10/20 second on/off cycle at 10% amplitude. The lysate (**Figure 16**) was then centrifuged in an SS-34 rotor (Thermo Fisher SORVALL RC6+ Centrifuge) at 14,000 rpm for 45 minutes at 4°C.

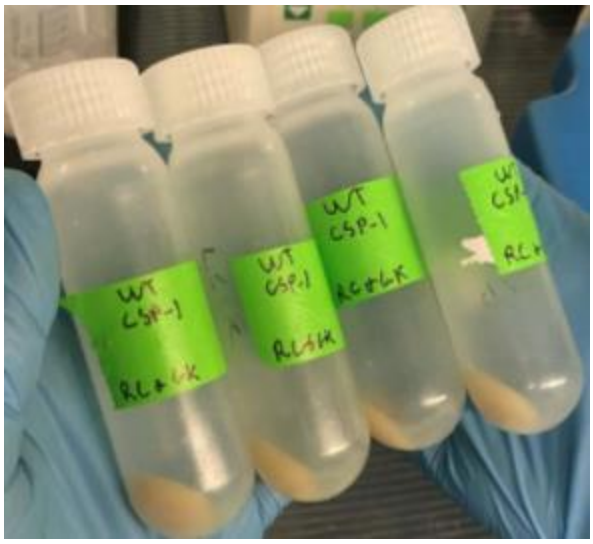

Figure 16: Representative centrifugation tubes used to contain lysate. Note the supernatant has been removed.

The supernatant was then filtered through a 0.45 μm filter and used for purification using a Strep-Tactin affinity column (GE Healthcare; **Figure 17**) pre-equilibrated with wash buffer (100 mM Tris, 150 mM NaCl, 1 mM EDTA, pH 8.0). The supernatant was loaded onto a 5 mL column at a flowrate of 4 mL/min using an Econo gradient pump (Bio-Rad; **Figure 17**) followed by washing with 20 mL of wash buffer to remove unbound proteins. The protein was eluted using 20 mL of elution buffer consisting of 100 mM pH 8.0 Tris-HCl, 150 mM NaCl, 1 mM EDTA, and 2.5 mM D-desthiobiotin (Sigma-Aldrich). The columns were regenerated using 10 mL of Milli-Q water followed by 16 mL of 0.5 M NaOH. The columns were then washed with 20 mL of Milli-Q water to remove the NaOH. Once the pH became neutral, the columns were stored back in the wash buffer.

Figure 17: Strep-Trap affinity column (left) and the Econo gradient pump (right) used and associated setup

Following affinity column purification, the protein was further purified by size exclusion chromatography (SEC). The protein was concentrated to 2 mL using 10 kDa MWCO filters (Millipore) centrifuged at 4000 rpm (Thermo Fisher Heraeus Megafuge 16R) and then filtered using a 0.22 μM filter (VWR). 1 mM (tris(2-carboxyethyl)phosphine) (TCEP; Goldbio) was added to the protein and loaded into an SEC column (GE Healthcare XK 16 High Load 16/60, Superdex 75, prep grade; **Figure 18**) with a 2 mL injection loop.

Figure 18: Size exclusion chromatography column used and associated setup

The purification was performed on an AKTA purifier 10 using elution buffer (50 mM Tris, 150 mM NaCl, pH 7.8) at a flow rate of 1 mL/min. The fraction corresponding to the protein peak (56−63 mL elution volume; **Figure 19**) was taken, and its concentration was determined using ε_{280} = 8480 $M^{-1}cm^{-1}$ and the Beer-Lambert Law (**Eq. 2**) where all variables correspond to values obtained at λ_{280}. A = absorbance, ε = molar extinction coefficient, c = concentration, and l = instrument pathlength.

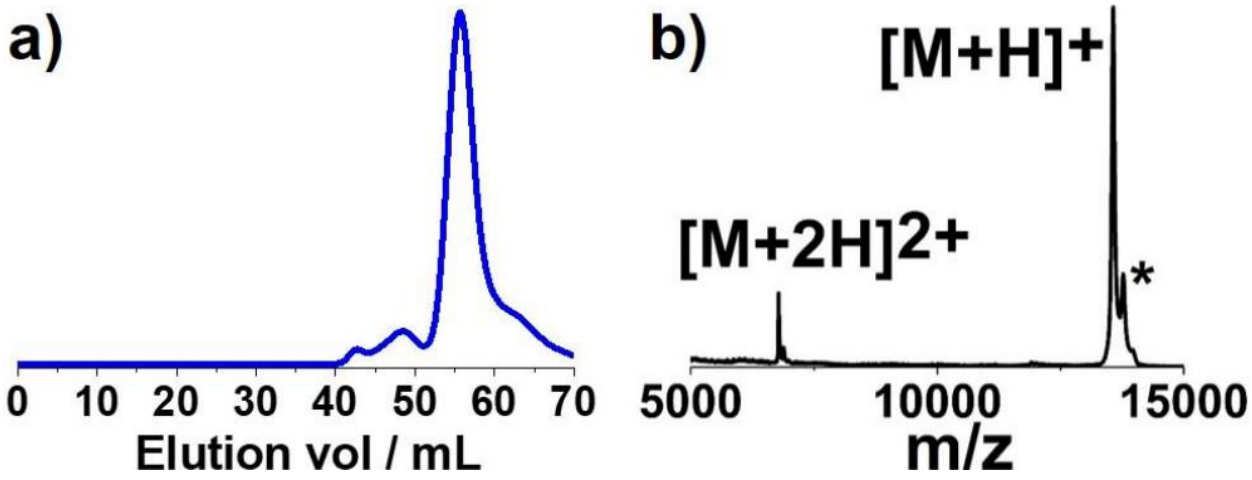

Figure 19: a) Size exclusion chromatogram of NBP purification showing the major peak corresponding to pure NBP with elution volume 56-63 mL. b) MALDI-MS of apo-NBP showing the correct identity of the protein (molecular ion peak observed at 13520 Da; calculated 13519 Da). The +224 Da peak marked with * is a non-specific adduct of the protein with sinapinic acid matrix.

$$A = \varepsilon cl \ldots\ldots\ldots \text{Eq. 2}$$

NBP's purification cycle takes 5 days. The Cys-free variant of NBP was expressed and purified to homogeneity using the same procedure as NBP's with a yield of approximately 13 mg/L of bacterial culture. The Cys-free protein's purity and mass were verified by SDS-PAGE and MALDI MS (observed 13,516 Da; calculated 13,518 Da), respectively as is seen in **Figure 20a** and **Figure 20b**.

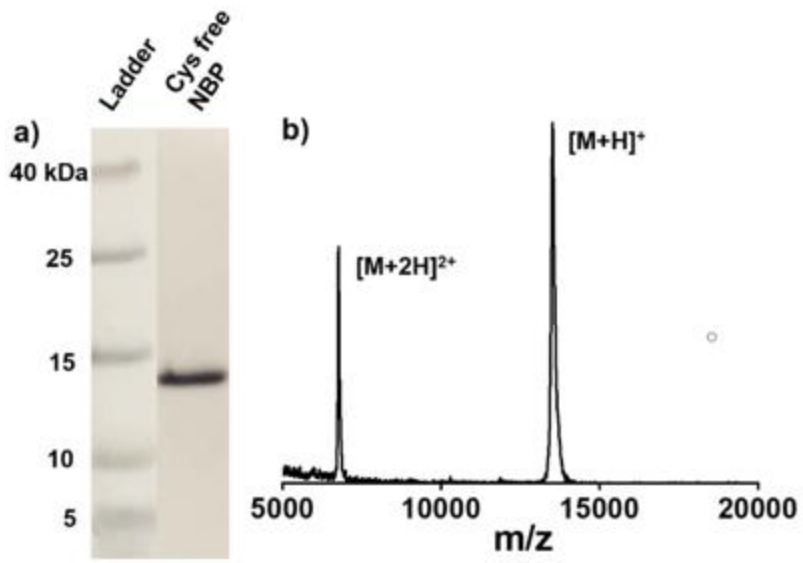

Figure 20: SDS-PAGE (a) and MALDI-MS (b) the Cys-free variant of NBP. The MALDI (observed 13516 Da; calc. 13518 Da) data was collected using sinapinic acid matrix.

2.3 Apo-NBP Crystallization

All crystallization occurred at ~20°C. First, a Pre-Crystallization Test (PCT) was performed to optimize the quantity of protein required for crystallization. Reagents were made to match those available in Hampton Research's HR2-140 commercial kit.[21] A protein concentration of 28 mg/mL was deemed most efficient from observations of PCT results. Following this, the sparse matrix reagent kits Crystal Screen 1 (HR2-110) and Crystal Screen 2 (HR2-112) (Hampton Research)[22] were used to determine crystallization conditions. Out of 98 condition sets tested, only one set yielded a crystal (**Figure 21a**) after one year of growth with the following conditions: 0.2 M ammonium sulfate, 0.1 M sodium acetate trihydrate (pH 4.6), 25% w/v polyethylene glycol (PEG) 4,000. This crystal, and all others in this work, were viewed by an Olympus SZH light microscope.

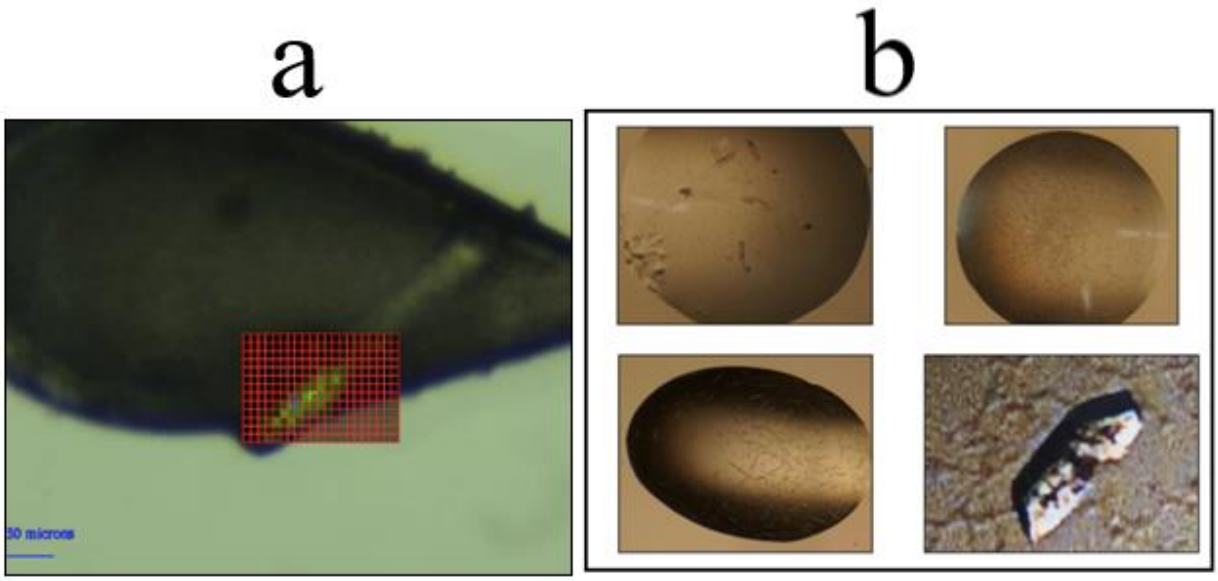

Figure 21: (a) apo-NBP crystal caught in an extraction loop. The red gridlines indicate the area used for x-ray diffraction. (b) apo-NBP crystals acquired via Bis-Tris screen tray

Additionally, considering the time required for the above crystallization to be successful, investigation into other viable condition sets was conducted. Based on successful crystallization attempts of apo-NBP's precursor apo-Csp1 in the literature,[23] similar screen conditions were established for apo-NBP. Of these conditions, the following screen offered the most developed results: 0.1 M Bis-Tris, PEG 3350 (22-27%), and pH (6.3-6.6). Final well volumes were 1 mL. All drops were created with a ratio of 1:1 protein solution to well solution. The protein concentration used was 25 mg/mL. This screen is simulated in **Figure 22**.

PEG 3350 Concentration (%)

pH	22	23	24	25	26	27
6.3	X		X			X
6.4		X	X			
6.5		X				X
6.6				X		X

Figure 22: A simulated view of tray conditions for apo-NBP crystallization. Each rectangle corresponds to a single well that possesses characteristics of the corresponding PEG and pH row and column respectively. Conditions where crystals developed are marked by an "X"

Both hanging and sitting drop models were capable of forming crystals under the same screen conditions. Some of the better developed crystals from this screen are provided in **Figure 21b**.

X-ray diffraction occurred at the Brookhaven National Lab's National Synchrotron Light Source II (NSLS-II) via the Frontier Microfocusing Macromolecular Crystallography (FMX) beamline. The diffraction pattern observed from the above crystals is shown in **Figure 23**.

Figure 23: The diffraction pattern for apo-NBP crystals observed. The intense, luminous dots of lights within the yellow oval correspond to relevant diffracted x-rays

A resolution of 2.8-3.0 Å was observed from collected data, and a structure for apo-NBP was created (**Figure 23**).

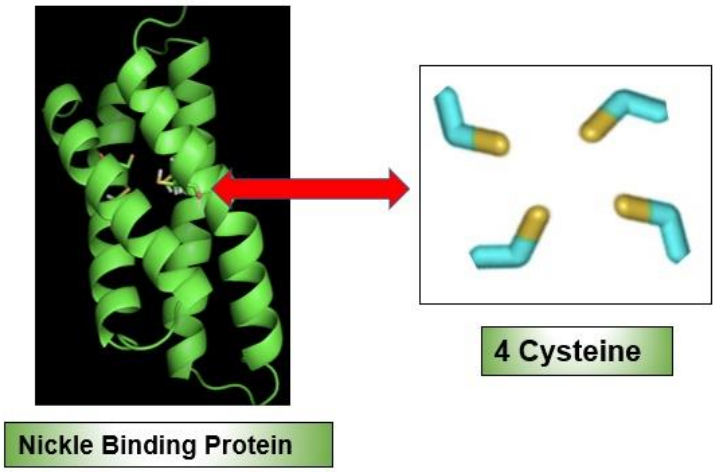

Figure 24: apo-NBP structure determined via data collected from x-ray diffraction of crystals retrieved from commercial crystal screen and Bis-Tris trays. Note the red arrow indicating the empty nickel binding site

The nickel binding site characteristic of the protein is visible as is its tetramer structure and α-helices. The model provided in **Figure 24** confirmed the successful redesign of Csp1 into NBP and the crystallization of its apo form.

2.4 Ni-NBP Crystallization

As of now, efforts to crystallize nickel-bound NBP (Ni-NBP) are directed toward condition optimization. Crystallization attempts have been made at both ~4°C and ~20°C. Guided by the success of crystallizing apo-NBP from conditions used for its protein pre-cursor, the literature was referenced again to determine appropriate conditions for Ni-NBP.[23] The conditions under optimization currently are as follows: 0.03 M $MgCl_2$, 0.03 M $CaCl_2$, 0.1 M Tris-Bicine pH 8.5, 12.5% v/v 2-methyl-2,4 pentanediol (racemic) plus 12.5% PEG 1000 and 12.5% PEG 3350. As with the apo-NBP screen trays, the pH and respective PEG concentrations are being varied. Optimization efforts include varying pH values from 8.0-8.7 at increments of 0.1, and the PEG concentrations from 11.5-16.5% at increments of 1.0%. The final well volume is 1 mL, and the drop ratio of protein solution to mother liquor is 1:1. Two equivalents of nickel are currently being introduced to the protein solutions. The protein concentrations under optimizations were 25 mg/mL and 28 mg/mL. These conditions are tabulated in screen format in **Figure 25**.

PEG 1000 & 3350 Concentrations (%)

pH	[Ni-NBP] = 25 mg/mL 2 Ni eq	11.5	12.5	13.5	14.5	15.5	16.5
	8.0						
	8.1						
	8.2						
	8.3						
	8.4						
	8.5						
	8.6						
	8.7						

PEG 1000 & 3350 Concentrations (%)

pH	[Ni-NBP] = 28 mg/mL 2 Ni eq	11.5	12.5	13.5	14.5	15.5	16.5
	8.0						
	8.1						
	8.2						
	8.3						
	8.4						
	8.5						
	8.6						
	8.7						

Figure 25: Conditions under optimization for Ni-NBP in screen format

If Ni-NBP crystals were to form for these conditions, they would be harvested and sent to Argonne National Laboratory for characterization.

Chapter 3: NBHP

3.1 NBHP Background

NBHP had different expression and purification procedures compared to NBP due to structural differences. NBHP, also known as Arabidopsis thaliana nitrobindin (At-Nb), possesses a β-barrel composed of ten antiparallel residue strands and is capable of binding nitric oxide (NO).[24,25] Due to identification of structural homologs of NBHP in *Mycobacterium tuberculosis*,

it is believed a novel family of NBHPs has potential to represent all β-barrel heme-binding proteins.[26] Visualizations relevant to NBHP are provided in **Figure 26**.

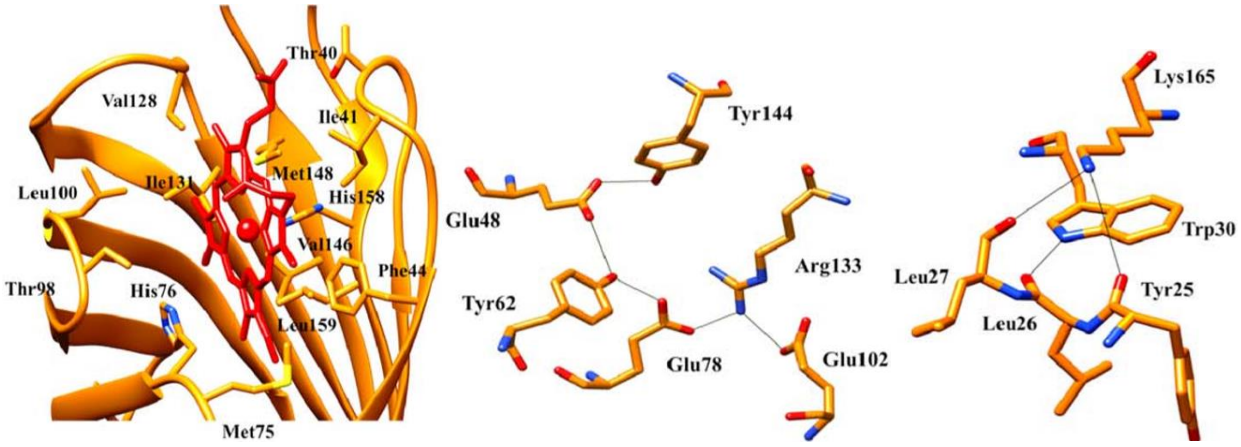

Figure 26: From left to right, models for NBHP's heme environment, central electrostatic network, and N-terminal electrostatic network are provided. Electrostatic interactions within a distance threshold of 3.5 Å are represented by continuous lines. The models were created with the UCSF-Chimera package[27]

3.2 NBHP Expression and Purification Procedure

The procedure for NBHP protein expression was as follows: A synthetic gene for Nitrobindin containing a N-terminal Strep-tag (WSHPQFEK) and a GGS spacer (Genscript) was cloned into a pET 29a (+) vector at the NdeI/NcoI restriction sites. The gene was dissolved at 100 ng/µL in Milli-Q water and stored at -20°C. In a pre-cooled 10 mL culture tube, 1 µL of gene and 50 µL of E.cloni EXPRESS DUOs BL21(DE3) chemically competent cells (Lucigen) were added and incubated in ice for 30 minutes. The cells were then subjected to heat shock at 42°C for 45 seconds and further incubated in ice for 10 minutes. Cell recovery was performed with 1 mL of LB media in an incubator-shaker (ThermoFisher MAXQ 4000) at 37°C for 1 hour. 50 µL of the cells were then plated on kanamycin LB agar plates and incubated at 37°C overnight. A 10 mL primary culture was inoculated with a freshly grown colony in LB media supplemented with 50 mg/mL kanamycin (Fisher) and was grown overnight at 180 rpm at 37°C. 1 L of kanamycin-supplemented secondary culture in LB media was inoculated with 10 mL of primary culture and

grown for 3-4 hours at 180 rpm at 37°C until the OD_{600} reached approximately 0.55. The culture was then induced with 0.5 mM (final concentration) of isopropyl β-D-1-thiogalactopyranoside (IPTG; Goldbio) and allowed to grow for 24 hours at 160 rpm at 30°C. The induced cells were harvested at 6000 rpm (SORVALL RC 5B PLUS) for 10 minutes and the pellets were stored overnight at -20°C.

The following day, the pellets were resuspended in 50 mL of lysis buffer comprised of 20 mM tris(hydroxymethyl)aminomethane (Tris-HCl; VWR) pH 8.5, 1 mM dithiothreitol (DTT; VWR), 1mM phenylmethane sulfonyl fluoride (PMSF; Biosynth Inc.), 1 mM EDTA, and 4 µL deoxyribonuclease (DNase I; ThermoFischer scientific.) followed by sonication on ice (Branson) for 3 minutes using a 10/20 second on/off cycle at 10% amplitude. The lysate was then centrifuged in an SS-34 rotor (Thermo Fisher SORVALL RC6+ Centrifuge) at 14,000 rpm for 45 minutes at 4°C. The supernatant was filtered through a 0.45 µm filter and purified by a Strep-Tactin affinity column (GE Healthcare) pre-equilibrated with wash buffer (100 mM Tris, 150 mM NaCl, 1 mM EDTA, pH 8.0). The supernatant was loaded onto a 5 mL column at a flowrate of 4 mL/min using an Econo gradient pump (Bio-Rad) followed by washing with 25 mL of wash buffer. The protein was eluted using 8 mL of elution buffer (2.5 mM [final concentration] D-desthiobiotin in wash buffer; Sigma Aldrich). The column was regenerated by washing it with 25 mL of water followed by 15 mL of 0.5 M NaOH. The column was then washed with water until the pH became neutral at which point it was stored back in the wash buffer.

Regarding heme extraction, the purified NBHP was then exchanged in cold water using a PD10 column prior to diluting the protein to 25 µM. 2M HCl was added to the resulting solution so its concentration was 1% followed by addition of equal volume of methyl ethyl ketone (MEK). NBHP was left undisturbed for 10 minutes before the heme layer was extracted via glass pipette.

Two additional washes with MEK were conducted to ensure complete heme extraction. NBHP was then dialyzed in water overnight to discard excess MEK.

Following dialyzation, heme repacking was performed at 4°C. NBHP was diluted to 10 µM using 20 mM Tris buffer, and 10 mM heme stock was prepared in 66 mM NaOH. Repacking was done by adding 0.5 equivalents of heme to the NBHP solution whilst stirring 10 minutes per each half equivalent added until 2 equivalents of heme had been added. The protein was left to stir for about 2-3 hours after the final addition of heme to allow for complete repacking.

NBHP's induction efficiency and purity were checked using a 12% Tris-Tricine SDS-PAGE gel. 5 µL of loading dye was added to 20 µL of each sample and heated at 90°C for 10 minutes. 15 µL of each analyte was then loaded onto the gel against a high molecular weight protein ladder and run at 100 V for 3 hours in a water circulated electrophoresis chamber (Thermo Fisher). The resulting gel (**Figure 27**) was stained in 0.3% coomassie blue solution composed of 45% methanol, 10% glacial acetic acid, 45% H_2O. The gel was destained in a solution composed of 30% methanol, 10% glacial acetic acid, and 60% H_2O.

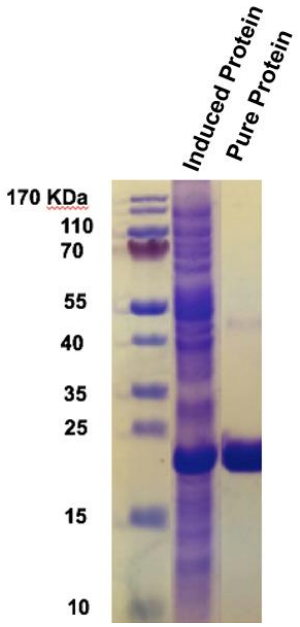

Figure 27: SDS-Page gel consisting of three (3) lanes. From the left, these lanes corresponded to the protein ladder, induced protein control, and purified protein

Chapter 4: BSA

4.1 Background

Bovine serum albumin (BSA) is a ~66463 kDa globular protein found in cows. Apo-BSA has been successfully crystallized[28,29] and had its structure modeled (**Figure 28**), but structure when bound to gold have not been reported.

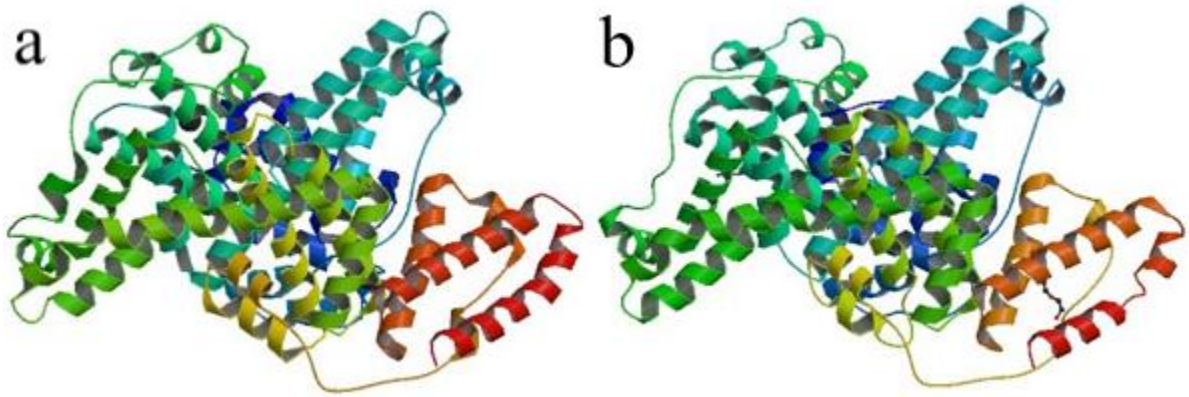

Figure 28: Literature structures of BSA from different studies. PDB codes for each structure are (a) = 3V03 and (b) = 4F5S. Resolution for (a) and (b) were 2.7 Å and 2.47 Å respectively.

Despite it already being crystallized, attempts to crystallize apo-BSA were made in this work to check reproducibility of the methods described in the literature.

4.2 Purification Procedure

The protocol for BSA purification was similar to NBP's SEC purification step. BSA (VWR) was dissolved in 50 mM Tris, 150 mM NaCl, pH 7.8 buffer then concentrated protein to 2 mL using 10 kDa MWCO filters (Millipore) centrifuged at 4000 rpm (Thermo Fisher Heraeus Megafuge 16R). The resulting solution was then sieved through a 0.22 μM filter (VWR). 1 mM tris(2-carboxyethyl)phosphine (TCEP; Goldbio) was added to the protein and loaded into an SEC column (GE Healthcare XK 16 High Load 16/60, Superdex 75, prep grade; **Figure 18**) with a 2 mL injection loop. The purification was performed on an AKTA purifier 10 using elution buffer (50 mM Tris, 150 mM NaCl, pH 7.8) at a flow rate of 1 mL/min. The fraction corresponding to

the protein peak (56−63 mL elution volume) was taken, and its concentration was determined using ε_{280} = 43824 $M^{-1}cm^{-1}$ and the Beer-Lambert Law (**Eq. 2**). The purified protein was stored at −80°C.

4.3 Apo-BSA Crystallization

Current efforts to crystallize apo-BSA are directed toward condition optimization. All crystallization occurred at room temperature (~20°C). Guided by success in the literature,[28,29] condition screens have been developed. The conditions under optimization currently are as follows: 0.2 M calcium acetate, 20% (w/v) PEG 3350, and 0.1 M Tris HCl pH 6.5 – henceforth "Condition Set A". Optimization efforts include varying Condition Set A's pH from 6.3-6.6 at intervals of 0.1, and its precipitant (PEG 3350) concentration from 17-22% at intervals of 1%. Condition Set A's protein solution concentration, originally reported as 10 mg/mL,[28] has been extrapolated into three separate concentrations: 10 mg/mL, 20 mg/mL, and 30 mg/mL. The final well volume is 1 mL, and the drop ratio of protein solution to mother liquor is 1:1. These conditions are simulated in screen format in **Figure 29**.

PEG 3350 Concentration (%)

[BSA] = 10 mg/mL	17	18	19	20	21	22
6.3						
6.4						
6.5						
6.6						

pH

PEG 3350 Concentration (%)

[BSA] = 20 mg/mL	17	18	19	20	21	22
6.3						
6.4						
6.5						
6.6						

pH

PEG 3350 Concentration (%)

[BSA] = 30 mg/mL	17	18	19	20	21	22
6.3						
6.4						
6.5						
6.6						

pH

Figure 29: Simulations for apo-BSA crystallization setups. Each rectangle corresponds to a single well that possesses characteristics of the corresponding PEG and pH row and column respectively. The protein concentrations used for those respective screens are provided in the tables' upper-leftmost corner.

Out of the conditions tested in **Figure 29**, crystals have been observed at a 10 mg/mL protein concentration where the pH was 6.3 and the PEG 3350 concentrations were 19-22% (**Figure 30**), but their lack of three-dimensional morphology resulted in them being unviable for x-ray diffraction techniques (**Figure 31**).

PEG 3350 Concentration (%)

[BSA] = 10 mg/mL	17	18	19	20	21	22
6.3			X	X	X	X
6.4						
6.5						
6.6						

pH

Figure 30: A simulated view of tray conditions for apo-BSA crystallization at [BSA] = 10 mg/mL. Each rectangle corresponds to a single well that possesses characteristics of the corresponding PEG and pH row and column respectively. Conditions for which crystals developed are marked by an "X"

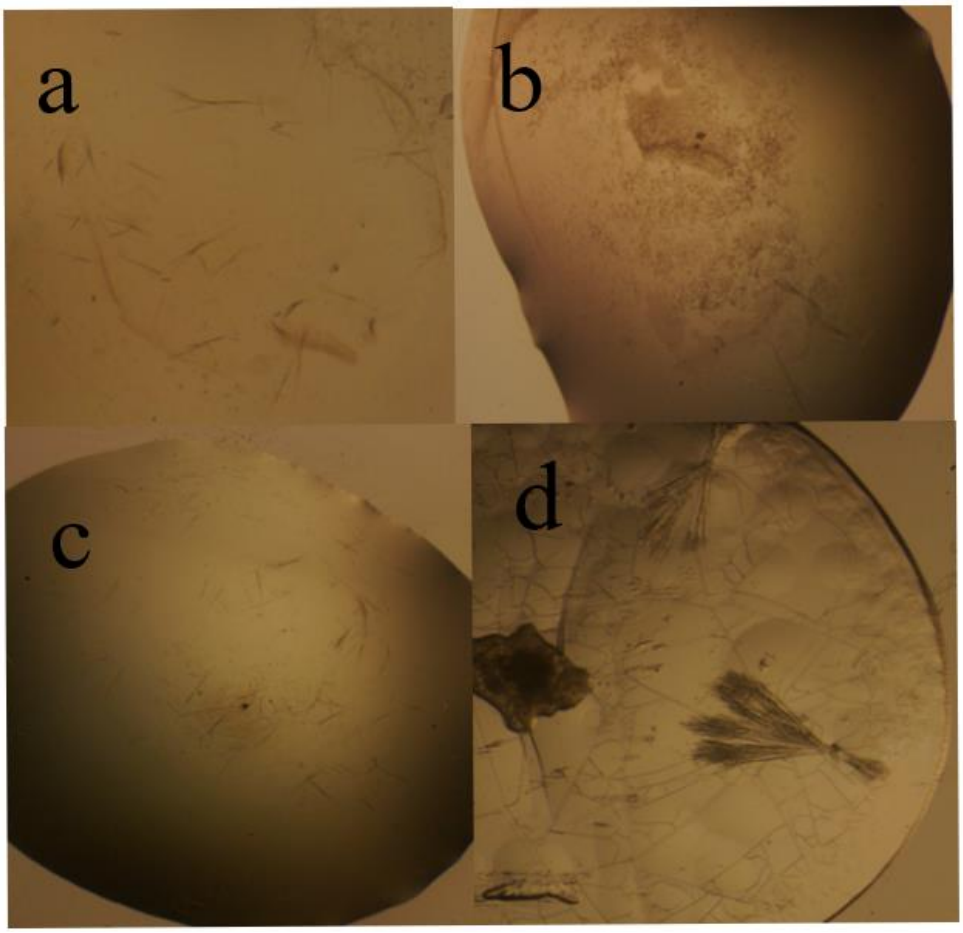

Figure 31: Apo-BSA crystals acquired from Crystal Set A. pH was 6.3 for each drop. PEG concentrations for each drop were as follows: (a) 19%, (b) 20%, (c) 21%, (d) 22%

As seen in **Figure 30**'s pictures, (a) and (c) contain thin needle-like formations, (b) possesses a large number of microcrystals, and (d) possesses needle clusters. Each of these crystals lacks the optimized depth (i.e. number of lattice planes) needed for x-ray diffraction. This could be due to the PEG 3350 concentration being too low causing the diffusion rate to be insufficient to stimulate crystal growth to the degree desired. Regardless of the experimental condition, BSA crystallization is considerably more difficult given its larger molecular weight (~66,463 kDa) and corresponding complexity to other proteins in this work, so continued condition optimization is required. Much like Ni-NBP, if better crystals were to form, they would be taken to Argonne National Laboratory for x-ray diffraction and structure elucidation.

4.4 Au-BSA Crystallization

Current efforts to crystallize Au-BSA are directed toward condition optimization. All crystallization occurred at room temperature (~20°C). Guided by success in the literature,[28,29,30] condition screens have been developed. The conditions under optimization currently are as follows: 22%(w/v) PEG 5000, 0.3 M NH_4Cl, and 0.1 M MES pH 6.5 – henceforth "Condition Set B".

Optimization efforts include varying Condition Set B's pH from 6.3-6.6 at intervals of 0.1, and its precipitant (PEG 5000) concentration from 20-25% at intervals of 1%. Condition Set B's protein solution concentration, originally reported as an unspecific range of 40-120 mg/mL,[29] has been extrapolated into five separate concentrations: 40 mg/mL, 60 mg/mL, 80 mg/mL, 100 mg/mL, and 120 mg/mL. 10 equivalents of chloroauric acid ($HAuCl_4$) was added to the Condition Set B's protein solution. The final well volume is 1 mL, and the drop ratio of protein solution to mother liquor is 1:1. These conditions are simulated in screen format in **Figure 32**.

Figure 32: Simulations for Au-BSA crystallization setups. Each rectangle corresponds to a single well that possesses characteristics of the corresponding PEG and pH row and column respectively. The protein concentrations used for those respective screens are provided in the tables' upper-leftmost corner, as are the Au equivalents.

Out of the conditions tested in **Figure 32**, no crystals have been observed for any of the well conditions regardless of protein concentration including those of Condition Set B; however, precipitation has been observed as has a violet coloration in the drop solution (**Figure 33**).

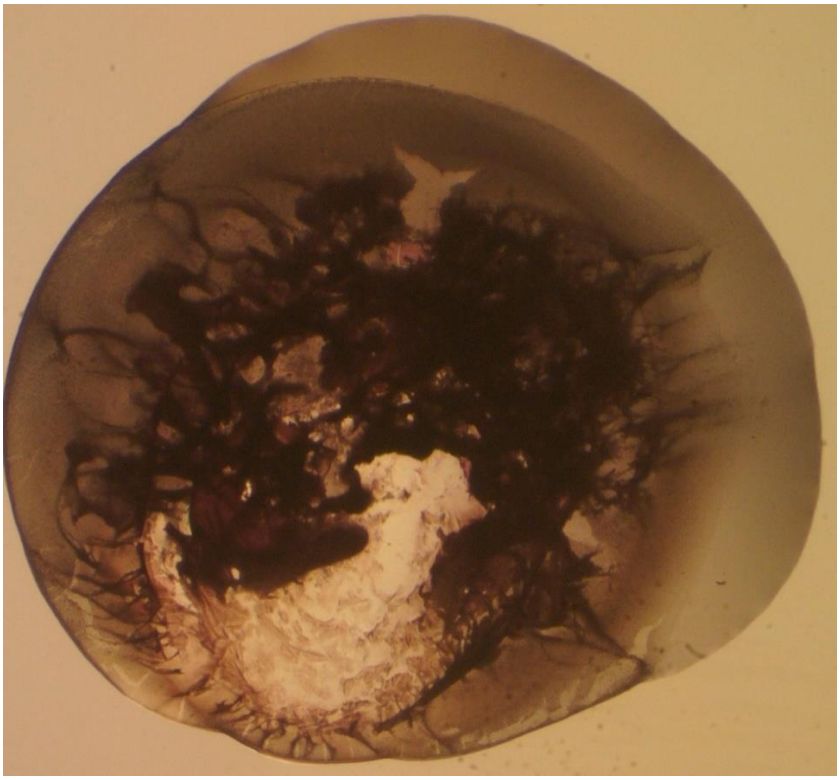

Figure 33: Representative sample of Au-BSA drop. Note the development of a skin around the drop's circumference and the violet precipitate's nebula-like structure. These characteristics are noted in each well system regardless of condition change

This color is believed to be caused by the Tris buffer reducing the gold in solution. Regardless, the existence of precipitate suggests either the protein concentration or salt concentration is too high, so lower concentrations for both of these variables are potential avenues of future crystallization attempts. As of yet, a viable crystal has not been developed, though if they were, they would be taken to Argonne National Laboratory for x-ray diffraction and structure elucidation.

Chapter 5: De Novo Tetramer

5.1 Background

The de novo tetramer is an attempt to expand comprehension of protein structures by exploring the characteristics of an artificially-designed α-helical tetramer barrel. This exploration's main aim is to rely on the known sequence-to-structure relationships of the α-helical coiled coil[31,32] to further knowledge of peptide engineering so as to inform future research efforts in the determination of potential applications in the fields of synthetic biology or biotechnology. Additionally, this α-helical tetramer's interactions with transition metals nickel and iron are also investigated.

A discussion of protein structure is required to understand this section. Proteins are composed of amino acids chained together by condensation reactions to form peptide bonds which cumulatively comprise a chain of amino acids also known as a peptide's primary sequence, an example of which is visualized in the synthesis of the tripeptide Glycine-Glycine-Glycine (**Figure 34)**.[33]

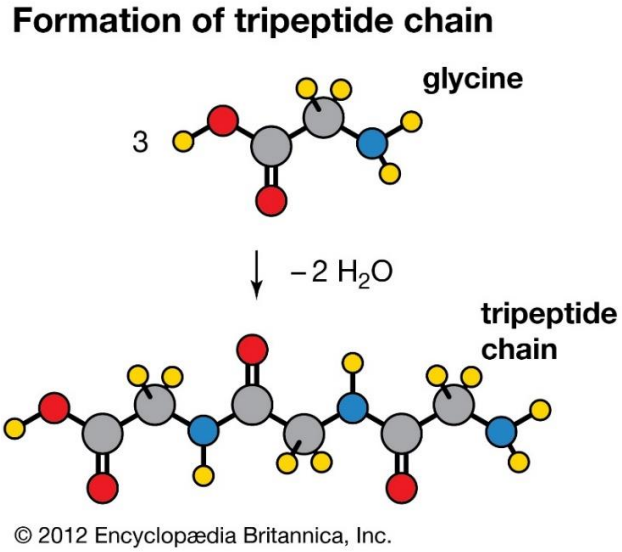

Figure 34: Shown is the binding of three glycine residues together to create a tripeptide. Formation causes the expulsion of two water molecules in two instances of one hydrogen from an amine group and one hydroxyl from a carboxylic acid group. In the figure, hydrogens are yellow, carbons are grey, oxygens are red, and nitrogens are blue.

As more amino acids are chained together, the peptide backbone's amino hydrogens and carbonyl oxygens may interact through hydrogen bonding to form α-helices, β-pleated sheets, β-turns, or Ω-coils, collectively known as secondary structures, of which the former is pertinent to this work.

The use of coiled-coil α-helices is due to a greater degree of comprehension regarding their sequence-to-structure relationships. This comprehension arrives as a pattern of hydrophilic (P) and hydrophobic (H) residues typically in a seven-unit heptad repeat $(HPPHPPP)_n$ which can also be denoted as *abcdefg* and visualized as a helical wheel (**Figure 35**).[34]

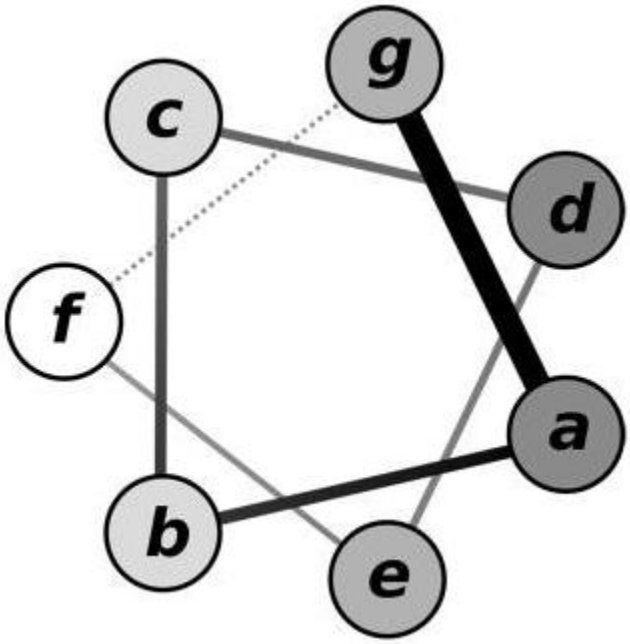

Figure 35: Helical wheel representation of heptad repeat sequence *abcdefg* displaced around an α-helix. Residues that are nearer to the helix interfaces are shaded more darkly

Additionally, α-helices with this heptad repeat demonstrate intramolecular interactions through sidechains known as knob-into-holes (KIH) packing with other α-helices of the same heptad repeat.[34,35] Combined, KIH packing and the heptad repeat provide a foundation from which these coiled-coil α-helices can be computationally[35,36,[x],37] and rationally designed.[38,39]

As this applies to this work, THE DE NOVO TETRAMER's α-helices are 30 residues long with a molecular weight 3301.91 g/mol and a theoretical pI of 6.36. It is overall composed of four α-helices arranged about a central axis to create an inner region of open space which may be used for metal binding. The de novo tetramer's primary sequence contains two Cys residues which when utilized in conjunction with the protein's tetramer structure results in eight Cys residues arranged in a metal-binding pocket similar theoretically in functionality to NBP. SC01's primary sequence is **Ac-GLAAIEQKCEACEKKLEAIEKKLAAIEWKG-CONH$_2$**, its helical wheel is represented in **Figure 36**, and 3D models of the protein's tertiary structure and Cys pocket spacing are visualized in **Figure 37a** and **Figure 37b** respectively.

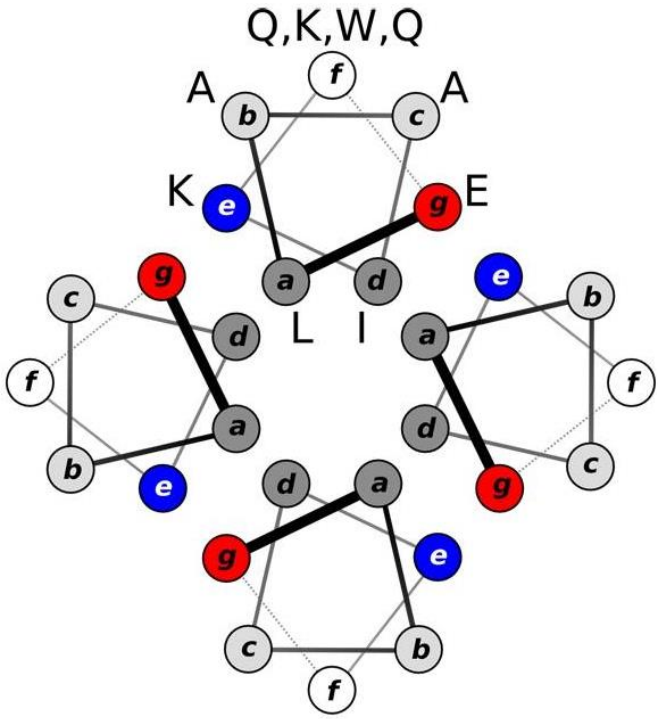

Figure 36: De novo tetramer helical wheel

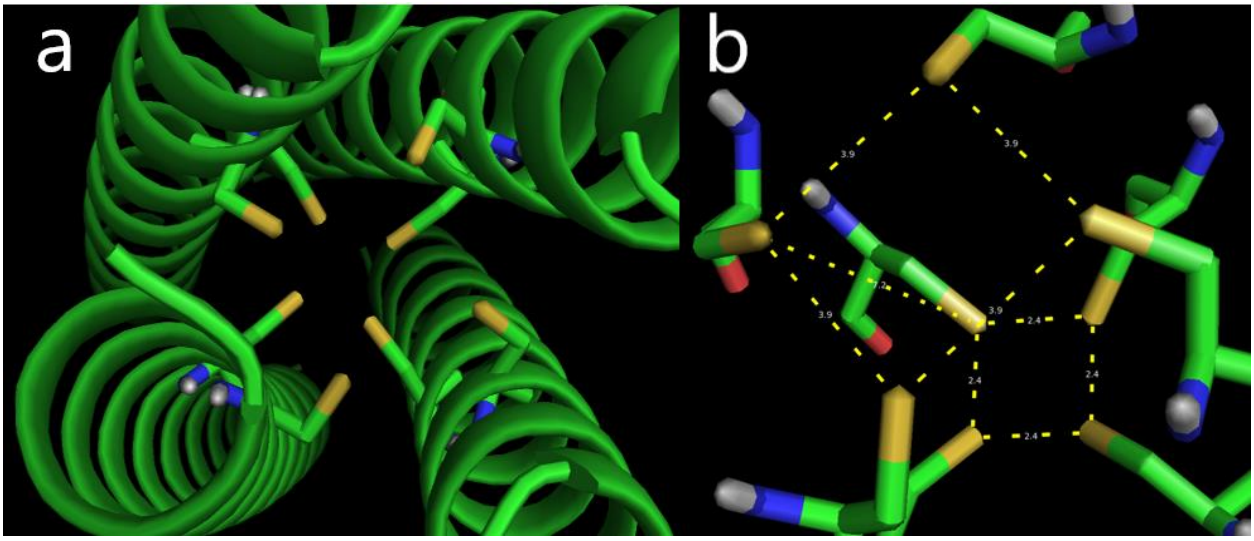

Figure 37: (a) CS-01's four α-helices arranged so their individual Cys residues form a central pocket for potential transition metal binding. (b) The Cys binding pocket with atomic distances in Å. Note the equally-spaced squares of edge length 3.9 Å and 2.4 Å respectively

5.2 Synthesis and Purification Procedure

Peptide synthesis was done by standard Fmoc SPPS protocols on a CEM LibertyBLUE microwave-assisted automated peptide synthesizer (CEM Corporation, Buckingham, UK). Peptides were synthesized on a Rink amide ChemMatrix resin (PCAS Biomatrix, Quebec, Canada) by taking advantage of HBTU activation. After automated synthesis, peptide acetylation using acetic anhydride and pyridine in DMF was performed. The crude peptide was then cleaved from the resin by treatment with a 95:2.5:2.5 mix of trifluoroacetic acid:water:triisopropylsilane for 2 hours at room temperature. The cleavage mixture was then dripped into ten times the volume of 0°C diethyl ether, and the precipitate that formed was isolated by centrifugation. The solid was dissolved in a 1:1 mix of water and acetonitrile and freeze-dried to give the crude peptide. This material was purified using reversed-phase HPLC using a C18 column (10 × 150 mm, Kromatek, UK) and running a gradient from 20 % to 80 % acetonitrile in water over 30 minutes.

5.3 Crystallization

De Novo Tetramer

Current efforts to crystallize the de novo tetramer are directed toward condition optimization. All crystallization occurred at room temperature (~20°C). Guided by success in the literature,[40,41] condition screens have been developed. The conditions under optimization currently are as follows: 1) 1.26M Ammonium sulfate and 0.1 M Tris pH 8.2-8.7 and 2) 25 mM imidazole pH 6.9-7.2, PEG 8000 20-25%, and 14.3% ethanol henceforth Condition Set C and Condition Set D respectively. Optimization efforts include varying the pH of both condition sets by intervals of 0.1, and its precipitant (PEG 8000) concentration, when applicable, at intervals of 1%. The peptide concentrations tested have been 10 mg/mL and 20 mg/mL for both condition sets. The final well volume is 1 mL, and the drop ratio of protein solution to mother liquor is 1:1. These conditions are simulated in screen format in **Figure 38**.

PEG 8000 Concentrations (%)

pH	[de novo] = 10 mg/mL	20	21	22	23	24	25
	6.9						
	7.0						
	7.1						
	7.2						

PEG 8000 Concentrations (%)

pH	[de novo] = 20 mg/mL	20	21	22	23	24	25
	6.9						
	7.0						
	7.1						
	7.2						

Ammonium Sulfate

pH	[de novo] = 10 mg/mL	1.26 M					
	8.2						
	8.3						
	8.4						
	8.5						
	8.6						
	8.7						

Ammonium Sulfate

pH	[de novo] = 20 mg/mL	1.26 M					
	8.2						
	8.3						
	8.4						
	8.5						
	8.6						
	8.7						

Figure 38: Conditions under optimization for the de novo tetramer in screen format

Out of these screens, a single well from Condition Set D yielded crystals (**Figure 39**).

Ammonium Sulfate

pH	[de novo] = 10 mg/mL	1.26 M					
	8.2						
	8.3						
	8.4						
	8.5		X				
	8.6						
	8.7						

Figure 39: A simulated view of tray conditions for de novo crystallization. Each rectangle corresponds to a single well that possesses characteristics of the corresponding PEG and pH row and column respectively. Conditions where crystals developed are marked by an "X"

These crystals are pictured in **Figure 40**.

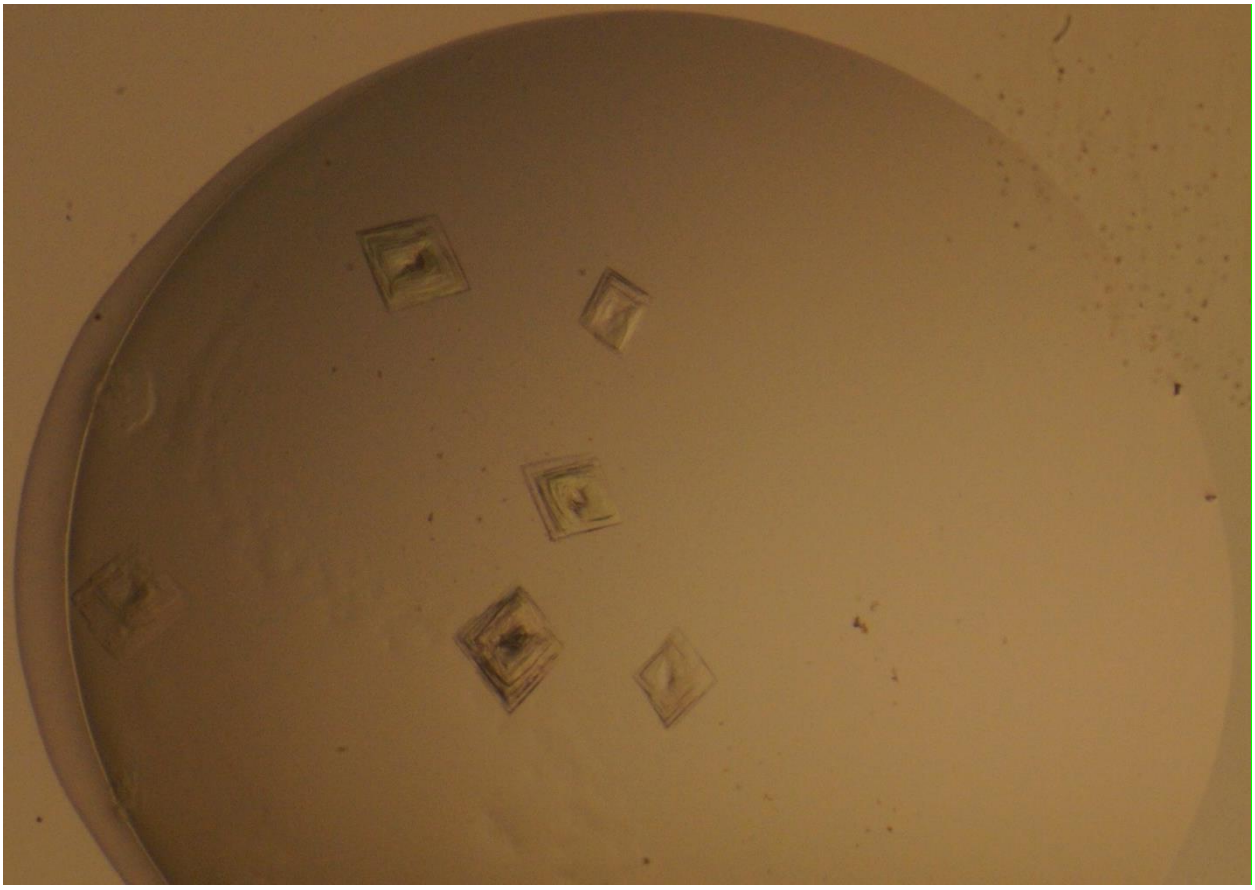

Figure 40: De novo tetramer crystals formed from Condition Set D

Note the crystals' square-like shape, sharp edges, concentric rings indicating 3D structure, and size relative to more granular precipitate indicating successful crystal formation. As crystals formed, they are to be taken to Argonne National Laboratory for x-ray diffraction and structure elucidation later in April.

Chapter 6: Conclusion

6.1 Conclusion

In summary, Crystals were successfully formed for apo-NBP and the de novo tetramer. The apo-NBP's crystal was analyzed via crystal diffraction techniques from which data was extracted so a 3D structure could be made. The de novo tetramer crystal will be exposed to crystal

diffraction techniques later in April at the Argonne National Laboratory where, if the crystals prove to be of sufficient quality, a 3D structure may be determined for it also. Further optimization must take please for Ni-NBP, apo-BSA, and Au-BSA crystal screen conditions. While crystals were observed for apo-BSA, their lack of 3D structure rendered them unviable for crystal diffraction efforts. Au-BSA screens, the ample presence of precipitate likely indicates protein concentrations under optimization are too large and that lowering these concentrations would yield more quantifiable results. Also, a change in the buffer used for the mother liquor may be required to prevent gold reduction and the subsequent violet coloration observed from said reduction. As for Ni-NBP, the lack of crystal formation could have resulted from numerous factors from protein's concentration being too low to interference from the nickel in solution, though the complex nature of protein crystallization still allows for the conditions under consideration to be potentially viable. It could be that these efforts just require more time to be brought to fruition.

List of References

[1] McPherson, A., & Gavira, J. A. (2014). Introduction to protein crystallization. *Acta Crystallographica Section F, 70*(1), 2-20. doi:10.1107/S2053230X13033141

[2] Britannica. https://www.britannica.com/science/Bragg-law

[3] Fierer, N., & Jackson, R. B. (2006). The diversity and biogeography of soil bacterial communities. *Proceedings of the National Academy of Sciences of the United States of America, 103*(3), 626-631. doi:10.1073/pnas.0507535103

[4] Anfinsen, C. B. (1973). Principles that govern the folding of protein chains. *Science, 181*(4096), 223-230. doi:10.1126/science.181.4096.223

[5] McPherson, A., Malkin, A. J., & Kuznetsov, Y. G. (2000). atomic force microscopy in the study of macromolecular crystal growth. *Annual Review of Biophysics and Biomolecular Structure, 29*(1), 361-410. doi:10.1146/annurev.biophys.29.1.361

[6] Watson, H., & Kendrew, J. (1976). the stereochemistry of the protein myoglobin. https://doi.org/10.2210/pdb1mbn/pdb

[7] Kuznetsov, Y. G., Malkin, A. & McPherson, A. (1998). atomic force microscopy studies of phase separations in macromolecular systems. *Phys. Rev. B*, 58, 6097–6103.

[8] Britannica. https://www.britannica.com/science/Bragg-law#/media/1/76973/17859

[9] Jancarik, J., & Kim, S. - . (1991). Sparse matrix sampling: A screening method for crystallization of proteins. *Journal of Applied Crystallography, 24*(4), 409-411. doi:10.1107/S0021889891004430

[10] Malkin, A. J., YuG, K., Land, T. A., DeYoreo, J. J., & McPherson, A. (1995). Mechanisms of growth for protein and virus crystals. *Nature Structural Biology, 2*(11), 956.

[11] De Simone, G., Ascenzi, P., & Polticelli, F. (2016). Nitrobindin: An ubiquitous family of all β- Barrel Heme- proteins. *IUBMB Life, 68*(6), 423-428. doi:10.1002/iub.1500

[12] Harbury, P. B., Plecs, J. J., Tidor, B., Alber, T., & Kim, P. S. (1998). High-resolution protein design with backbone freedom. *Science, 282*(5393), 1462-1467.

[13] Piazza, R. (1999). Interactions in protein solutions near crystallisation: A colloid physics approach. *Journal of Crystal Growth, 196*(2), 415-423. doi:10.1016/S0022-0248(98)00867-7

[14] Pieter Rein ten Wolde, & Frenkel, D. (1997). Enhancement of protein crystal nucleation by critical density fluctuations. *Science, 277*(5334), 1975-1978. doi:10.1126/science.277.5334.1975

[15] Kogoy, J. M. (2003). *Protein Crystallization*. Retrieved from http://bio.davidson.edu/courses/MolBio/MolStudents/spring2003/Kogoy/protein.html

[16] Covington, R. (2019). *Studies on Luminescent Gold and Platinum Nanoclusters for Biological Sensing and Catalysis*. Retrieved from http://thesis.honors.olemiss.edu/1389

[17] Abbas, M. A., Kamat, P. V., Bang, J. H., & Univ. of Notre Dame, IN (United States). (2018). Thiolated gold nanoclusters for light energy conversion. *ACS Energy Letters, 3*(4), 840-854. doi:10.1021/acsenergylett.8b00070

[18] Chen, L., Wang, C., Yuan, Z., & Chang, H. (2015). Fluorescent gold nanoclusters: Recent advances in sensing and imaging. *Analytical Chemistry, 87*(1), 216-229. doi:10.1021/ac503636j

[19] Selvan, D., Prasad, P., Farquhar, E. R., Shi, Y., Crane, S., Zhang, Y., & Chakraborty, S. (2019). Redesign of a copper storage protein into an artificial hydrogenase. *ACS Catalysis, 9*(7), 5847-5859. doi:10.1021/acscatal.9b00360

[20] Selvan, D., Shi, Y., Prasad, P., Crane, S., Zhang, Y., & Chakraborty, S. (2020). The oxygen reactivity of an artificial hydrogenase designed in a reengineered copper storage protein. *Dalton Transactions (Cambridge, England : 2003), 49*(6), 1928-1934. doi:10.1039/C9DT04913D

[21] Hampton Research. (2019). *Pre-Crystallization Test*. Retrieved from https://hamptonresearch.com/uploads/support_materials/HR2-140_142_UG.pdf

[22] Hampton Research. (2019). *Crystal Screen 2* [PDF]. Retrieved from https://hamptonresearch.com/uploads/support_materials/HR2-112_binder.pdf

[23] Vita, N., Platsaki, S., Baslé, A., Allen, S. J., Paterson, N. G., Crombie, A. T., . . . Dennison, C. (2015). A four-helix bundle stores copper for methane oxidation. *Nature, 525*(7567), 140-143. doi:10.1038/nature14854

[24] Bianchetti, C. M., Blouin, G. C., Bitto, E., Olson, J. S., Phillips, G. N., & Argonne National Lab. (ANL), Argonne, IL (United States). Advanced Photon Source (APS). (2010). The structure and NO binding properties of the nitrophorin- like heme- binding protein from arabidopsis thaliana gene locus At1g79260.1. *Proteins: Structure, Function, and Bioinformatics, 78*(4), 917-931. doi:10.1002/prot.22617 [25] Grigoryan, G., Reinke, A. W., & Keating, A. E. (2009). Design of protein-interaction specificity gives selective bZIP-binding peptides. *Nature, 458*(7240), 859-864. doi:10.1038/nature07885

[26] Bianchetti, C. M., Bingman, C. A., Phillips, G. N., & Argonne National Lab. (ANL), Argonne, IL (United States). Advanced Photon Source (APS). (2011;2012;). Structure of the C-terminal heme- binding domain of THAP domain containing protein 4 from homo sapiens. *Proteins: Structure, Function, and Bioinformatics, 79*(4), 1337-1341. doi:10.1002/prot.22944

[27] Nautiyal, S., Woolfson, D. N., King, D. S., & Alber, T. (1995). A designed heterotrimeric coiled coil. *Biochemistry, 34*(37), 11645-11651. doi:10.1021/bi00037a001

[28] Majorek, K. A., Porebski, P. J., Dayal, A., Zimmerman, M. D., Jablonska, K., Stewart, A. J., . . . Minor, W. (2012). Structural and immunologic characterization of bovine, horse, and rabbit serum albumins. *Molecular Immunology, 52*(3-4), 174-182. doi:10.1016/j.molimm.2012.05.011

[29] Bujacz, A. (2012). Structures of bovine, equine and leporine serum albumin. *Acta Crystallographica Section D, 68*(10), 1278-1289. doi:10.1107/S0907444912027047

[30] Selvan, D., Prasad, P., Crane, S., Abuhagr, A., Covington, R., Artyushkova, K., Ramakrishna, G., & Chakraborty, S. (2019). Intrinsically fluorescent gold nanoclusters stabilized within a copper storage protein that follow the Irving–Williams trend in metal ion sensing. *The Analyst*, *144*(13), 3949-3958. https://doi.org/10.1039/c9an00426b

[31] Mason, J. M., & Arndt, K. M. (2004). Coiled coil domains: Stability, specificity, and biological implications. *Chembiochem*, *5*(2), 170-176. doi:10.1002/cbic.200300781

[32] Parry, D. A. D., Fraser, R. D. B., & Squire, J. M. (2008). Fifty years of coiled-coils and α-helical bundles: A close relationship between sequence and structure. *Journal of Structural Biology*, *163*(3), 258-269. doi:10.1016/j.jsb.2008.01.016

[33] Reddy, M. K. (2019, July 17). *Amino acid*. Encyclopedia Britannica. https://www.britannica.com/science/amino-acid

[34] Crick FHC. The Packing of Alpha-Helices - Simple Coiled-Coils. Acta Crystallogr. 1953;6:689–697.

[35] Grigoryan, G., Kim, Y. H., Acharya, R., Axelrod, K., Jain, R. M., Willis, L., . . . DeGrado, W. F. (2011). Computational design of virus-like protein assemblies on carbon nanotube surfaces. *Science, 332*(6033), 1071-1076. doi:10.1126/science.1198841

[36] Grigoryan, G., & Keating, A. E. (2008). Structural specificity in coiled-coil interactions. *Current Opinion in Structural Biology*, *18*(4), 477-483. doi:10.1016/j.sbi.2008.04.008

[37] Pettersen, E. F., Goddard, T. D., Huang, C. C., Couch, G. S., Greenblatt, D. M., Meng, E. C., & Ferrin, T. E. (2004). UCSF Chimera—A visualization system for exploratory research and analysis. *Journal of Computational Chemistry*, *25*(13), 1605-1612. doi:10.1002/jcc.20084

[38] Grigoryan, G., & DeGrado, W. F. (2011). Probing designability via a generalized model of helical bundle geometry. *Journal of Molecular Biology, 405*(4), 1079-1100. doi:10.1016/j.jmb.2010.08.058

[39] Walshaw, J., & Woolfson, D. N. (2001). SOCKET: A program for identifying and analysing coiled-coil motifs within protein structures. *Journal of Molecular Biology, 307*(5), 1427-1450. doi:10.1006/jmbi.2001.4545

[40] W. F., Lovejoy, Raleigh, D. P., DeGrado, Betz, S. F, B., Anderson, D., Ogihara, N., & Eisenberg, D. (1996). Crystallization of a designed peptide from a molten globule ensemble. *Folding and Design*, *1*(1), 57-64. https://doi.org/10.1016/s1359-0278(96)00012-0

[41] Eisenberg, D., Wilcox, W., Eshita, S. M., Pryciak, P. M., Ho, S. P., & Degrado, W. F. (1986). The design, synthesis, and crystallization of an alpha- helical peptide. *Proteins: Structure, Function, and Bioinformatics, 1*(1), 16-22. doi:10.1002/prot.340010105